Astron. Astrophys. 331, 760–770 (1998)

ASTRONOMY AND ASTROPHYSICS

Hanle depolarisation in the solar chromosphere

M. Bianda[1], **S.K. Solanki**[2], **and J.O. Stenflo**[2]

[1] Istituto Ricerche Solari Locarno (IRSOL), Via Patocchi, CH-6605 Locarno-Monti, Switzerland
[2] Institute of Astronomy, ETH-Zentrum, CH-8092 Zürich, Switzerland

Received 17 April 1997 / Accepted 3 November 1997

Abstract. A new polarimeter and an extension of the polarimetric technique of Donati et al. (1990) to higher polarisation values are presented. With this system, which allows low-noise polarimetric observations in the blue and near-UV part of the solar spectrum, we have recorded more than 200 Q/I profiles of Ca I 4227 Å with an accuracy of 2–3$\times 10^{-4}$.

We find that while the Q/I line shape outside the line core is very stable from one part of the solar surface to the next, the line core exhibits large variations relative to the rest of the profile. These variations are best interpreted in terms of partial depolarisation produced by the Hanle effect in the presence of weak fields. We obtain a quantitative and model-independent estimate of the depolarisation, from which we deduce field strengths of 5–15 G at the level of line-core formation, i.e. in the low to mid chromosphere. We also find evidence that the field strength is distributed around these average values with a FWHM that is approximately the same as the average value.

Key words: polarization – scattering – polarimeter – polarimetric technique – Sun: magnetic field – Sun: chromosphere – Hanle effect

1. Introduction

Due to its versatility and relative ease of use the Zeeman effect has been the mainstay of observational investigations of solar magnetism, in particular of the intrinsically strong (kG) fields organized into the network, active-region plages and sunspots. The Zeeman effect suffers, however, from a lack of sensitivity to intrinsically weak fields and to fields with mixed polarities or random orientations at small scales (turbulent fields).

A promising alternative is the Hanle effect (Hanle 1924, Moruzzi & Strumia 1991, Stenflo 1994). It makes the polarization in appropriate spectral lines sensitive to very weak fields, and allows their strengths and directions to be determined. In addition, it can detect fields even when they are turbulent and hence practically invisible to the Zeeman effect. The Hanle effect has been employed to deduce the magnetic structure of solar prominences (Leroy et al. 1977, Sahal-Bréchot et al. 1977, Bommier 1980, Landi Degl'Innocenti 1982, Querfeld et al. 1985), turbulent fields in the solar photosphere (Stenflo 1982, Faurobert-Scholl 1993, Faurobert-Scholl et al. 1995) and magnetic canopies in the chromosphere (Faurobert-Scholl 1992, 1994). All in all, however, it has been employed relatively rarely. The problem has largely been an observational one, since the proper interpretation of the Hanle effect requires observations that combine high spectral resolution with high polarimetric accuracy. These conditions have recently been met by the Zurich Imaging Stokes Polarimeter (ZIMPOL; Povel 1995), which has opened new windows for the measurement of polarisation produced by resonant scattering (Stenflo & Keller 1996, 1997, Stenflo 1997, Stenflo et al. 1997). One shortcoming of the present version of ZIMPOL is that its detectors are insensitive to wavelengths below about 4500 Å. This is unfortunate, since most of the lines showing strong resonance polarisation, a prerequisite for Hanle depolarisation, are located in the blue or the UV.

In the present paper we briefly describe a simple polarimeter that allows us to obtain Q/I observations with noise levels in the continuum approaching 10^{-4} at wavelengths down to 3800 Å (Q is the net linear polarisation and I is the intensity). It opens up an interesting spectral region to accurate observations of resonance polarisation and possible Hanle depolarisation. We also present and analyse the first observations made with this instrument.

The spectral survey of resonance polarisation carried out by Stenflo et al. (1983a,b) showed that the Ca I 4227 Å resonance line has the strongest Q/I signature in the whole visible and near UV spectrum. This line has also been one of the most often observed, resonantly polarized spectral features (Brückner 1963, Stenflo 1974, Wiehr 1975, Stenflo et al. 1980). Coincidently, Brückner discovered the polarisation of this line with the same telescope with which our observations have been obtained. The line core is formed in the mid chromosphere (Faurobert-Scholl 1992), a height for which hardly any Zeeman-effect based diagnostics exist. Finally, through the Hanle effect it is sensitive to field strengths of about 5–100 G. This range corresponds to the field strengths expected in the mid chromosphere, in particular in the quiet sun. In the present paper we present Q/I observa-

tions of this line and analyse them in search for the signature of the Hanle effect.

The centre-to-limb variation (CLV) of the Stokes vector of this line was last recorded by Stenflo et al. (1980) with a noise level of approximately 0.1%. The main disadvantage of these observations is that the solar surface was sampled only at a few locations, so that it is unclear to what extent these data are representative of the quiet Sun. In addition, the spectral resolution was relatively low, although this may not be important for a broad line like Ca I 4227 Å. Based on these observations Faurobert-Scholl (1992, 1994) deduced that there is a magnetic field of 20–100 G at heights between 700 and 1200 km above the continuum-forming level, if she assumes that the field is in the form of a magnetic canopy, i.e., a horizontal magnetic field overlying a field-free atmosphere (cf. Giovanelli 1980).

In the present paper we analyse a large number of Stokes I and Q/I spectra of Ca I 4227 Å obtained in the quiet Sun with both low noise and high spectral resolution. The instrumental setup and observations are described in Sect. 2, the reduction technique in Sect. 3, the data analysis and results in Sect. 4. Finally, conclusions are drawn in Sect. 5.

2. Instrumentation and observations

2.1. Instrumental set-up

Observations were carried out with the now completely refurbished, evacuated Gregory-Coudé telescope and the Czerny-Turner spectrograph of IRSOL (Istituto Ricerche Solari Locarno) located above Locarno in Switzerland. The telescope has an aperture of 45 cm and a total focal length of 25 m, while the spectrograph has a focal length of 10 m and a grating with the dimensions 180 × 360 mm ruled at 300 l/mm with a blaze-angle of 63°. To keep different spectral orders from overlapping and minimize stray light a predisperser is used, placed immediately after the spectrograph slit (which has a width of 200 μm, corresponding to 1.65″). The telescope has optics that are almost identical to those of the Gregory-Coudé Telescope operated by Göttingen University on Tenerife. Except for two plane mirrors, all of the optical elements of the telescope are on-axis and should not produce any significant cross-talk between the Stokes parameters (if we disregard the entrance window). Due to the positioning of these two mirrors the instrumental polarisation does not vary during the day, but only with the Sun's declination. Around equinox the two off-axis mirrors, inclined by 45° to the beam, compensate each other, since their position angles are 90° apart (Martínez Pillet & Sánchez 1991). Thus at this time the telescope may be considered to be nearly polarisation-free (with the exception of the entrance window). All observations discussed in this paper were carried out near an equinox.

The detector used is a blue-enhanced CCD system with 400 × 600 pixels, each corresponding to 0.18″ × 2.8 mÅ at 4227 Å.

We follow the observational technique proposed and applied by Donati et al. (1990), Semel et al. (1993) and Semel (1994, 1995). A total of four spectral images of each observed solar region are obtained (composed of two simultaneous spectral image pairs). By constructing appropriate ratios between these images we can obtain very low noise levels in Q/I (approaching 10^{-4}). We employ a polarizing beamsplitter (a calcite polarizer) together with a manually rotated half-wave plate. The beamsplitter is placed a few cm in front of the spectrograph slit and is aligned (with the aid of pores and the solar limb) in such a way that it projects the same part of the solar surface twice onto the spectrograph slit (these two images correspond to the two polarisation components, which are aligned to better than 1″). The unvigneted part of each image covers 18″ on the solar surface.

The rotatable half-wave plate precedes the polarizing beamsplitter and can be set in two different orientations. In the first the fast axis is parallel to one of the axes of the polarizer, while in the other the half-wave plate is rotated by 45°, so that the Stokes co-ordinate system is rotated by 90°. In this manner the polarisation of the two images is exchanged.

Two CCD frames are stored at every observed solar location, one per half-wave plate orientation (which is rotated manually while the CCD is being read out and the data are being stored on disc). In order to avoid pixel misalignments care is taken to have the CCD pixels oriented parallel to the spectral dispersion and to have spectral lines exactly aligned with the pixel columns (telluric lines are used for this purpose).

We have verified the efficiency of the polarisation optics with the aid of a Glan Thompson polarizer. At three wavelengths of interest for resonance polarisation measurements, namely those of the Sr I 4607 Å, Ca I 4227 Å and Sr II 4077 Å lines, we find efficiencies of 99.5%, 98.8% and 97%, respectively. The reason for the decreasing efficiency towards the violet is that the achromatic half-wave plate is used outside its specified wavelength range (4600-6800 Å).

2.2. Observations

We observed the core and inner wings of the Ca I resonance line at 4227 Å on 12th, 14th, 17th and 20th October 1995, on 23rd, 26th, 28th and 29th March 1996 and on 12th April 1996. The complete wavelength range covered by one CCD setting was 4225.9–4227.4 Å. Since this is not enough to cover the central part of the line and at the same time also obtain a part of the neighbouring continuum we have in some cases made two recordings at the same spatial position, each at a different wavelength location. The recordings were carefully combined using the data points in the wavelength range in which they overlapped. It is necessary to have observations of the line core together with the continuum in order to determine the stray light and the zero level of the polarisation.

By constructing appropriate ratios between the set of four recorded images it is possible to obtain the fractional linear polarisation Q/I as a function of wavelength and spatial position almost free from gain table, plate transparency and seeing-induced spurious polarisation (see Sect. 3.2, Semel et al. 1993). A residual fixed-pattern Q/I background remains, however. It

can be removed by making additional recordings at disc centre, where for symmetry reasons the intrinsic scattering polarisation disappears, while the fixed spurious pattern remains unchanged. Thus we alternate recordings at positions near the limb (the actual measurements) with recordings at disc centre (calibrations).[1] Generally we carried out a measurement at disc centre after every third or fourth registration at the limb. To avoid the introduction of unwanted granular Doppler shifts or Zeeman signals from magnetic features the telescope was moved during exposures at disc centre.

A total of 207 solar regions were recorded at $\mu = \cos\theta$ values ranging between 0.8 and 0.05 (here θ is the heliocentric angle). An additional 60 recordings were also made at disc centre. Generally the full centre-to-limb variation (CLV) of Q/I was recorded. Only on 26th March 1996 did we confine ourselves to locations close to the solar limb ($0.05 < \mu < 0.15$). The aim in that case was to search for variations in Q/I at different positions along the limb.

Exposure times were typically 5 s at disc centre and 20 s at $\mu = 0.05$. Hence the total time needed to record and store a full set of measurements (i.e. an image pair near the limb and at disc centre) ranged between 350 sec and 500 sec (including moving the telescope and confirming the μ value), depending on the observed μ.

During all exposures at $\mu < 1$ the slit was placed parallel to the nearest part of the solar limb. Stokes Q is positive along the slit, i.e. parallel to the limb. In a Gregory-Coudé system the image rotates on the slit plane, so that at a given time only two parts of the solar limb (180° apart) can be observed due to this requirement. Conversely, a given part of the solar limb can be observed for a few minutes only. An optical image rotation compensator would have to be placed behind the polarimeter (but before the slit) to avoid excessive instrumental polarisation. Since, however, the beam splitter must be located close to a focus, an image rotator would require special transfer optics to reimage the focus placed near the beamsplitter onto the slit, and has consequently not been employed.

For $\mu \leq 0.3$ we determine the position of the slit by measuring its distance from the solar limb, whereas for $\mu > 0.3$ the guiding system is employed. Image motion, seeing and guiding errors limit the exact reproduction of the observed position between the two exposures to 1–3″ (depending mainly on seeing conditions).

[1] This procedure would in principle also permit us to follow the sky transparency evolution for a better determination of the μ-value. We found, however, that although such a procedure works for Sr I 4607 Å and Sr II 4077 Å, it is impracticable with our setup for large numbers of Ca I 4227 Å observations, due to the necessity of determining the continuum co-temporally in every case. We have consequently not made use of it in this paper.

3. Data reduction

3.1. Overview of the reduction procedure

The main steps of the data reduction are as follows: 1. Dark current subtraction; 2. Flat fielding (it is required only for Stokes I, since the technique of Donati et al. (1990) does not require flat fielding to obtain Q/I); 3. Extraction of Q/I from the observed frames (as described in Sect. 3.2); 4. Determination of spectral smearing and stray light, as well as removal of the latter from the data (Sect. 3.3); 5. Correction of the instrumental zero level and remaining fixed pattern noise using data obtained at disc centre (Sect. 3.4); and 6. Fourier smoothing to reduce noise in the data (Sect. 3.5).

3.2. Extraction of Q/I

3.2.1. Basic technique

Donati et al. (1990) and Semel et al. (1993) proposed that very low noise V/I measurements can be made without having to flat-field or worry about retarder transparency by a simple combination of a polarizing beamsplitter and a quarter-wave plate, which can be switched to provide $\pm\lambda/4$ retardation. We have applied this technique to determine Q/I using a half-wave plate. The following description is for Q/I measurements, but it is of course possible to apply this technique to Stokes V and U simply by changing the polarisation analysis accordingly. All the equations in this section apply equally to Stokes V and U if Stokes Q is replaced by the desired Stokes parameter.

By carrying out two measurements, one for each retarder setting, and forming

$$F = \frac{1}{2}\left(\frac{f_1^+ f_2^+}{f_1^- f_2^-} - 1\right), \tag{1}$$

one obtains a good approximation for Q/I averaged over both measurements that is free from effects of the detector gain table and half-wave plate transparency at the two settings. In Eq. (1) $f_{1,2}^{+,-}$ represent the four images (exposures 1 and 2, for the polarisation states denoted by + and −),

$$\begin{aligned} f_1^+ &= (I_1^l + Q_1^l + \delta_1^l) R_1 G_l, \\ f_2^+ &= (I_2^r + Q_2^r + \delta_2^r) R_2 G_r, \\ f_1^- &= (I_1^r - Q_1^r - \delta_1^r) R_1 G_r, \\ f_2^- &= (I_2^l - Q_2^l - \delta_2^l) R_2 G_l. \end{aligned} \tag{2}$$

Here $G_{l,r}$ is the detector gain on the left and right parts of the detector array, $R_{1,2}$ the throughput of the polarimeter at the two settings (e.g. due to mechanical misalignments, or if the half-wave plate is not perfect at the observed wavelength), $I_{1,2}$ the Stokes I signal of the two exposures, $Q_{1,2}$ the corresponding Stokes Q signal and

$$\delta_j = \delta_{Ij} I_j + \delta_{Vj} V_j + \delta_{Uj} U_j, \qquad j = 1, 2, \tag{3}$$

a term that takes into account telescopic cross-talk from Stokes I, Stokes V and Stokes U into Stokes Q. Such a term is generally present in solar observations, since most solar telescopes are not axially symmetric, and wavelength dependent V and U signals are produced by the Zeeman effect and – in the case of U – by the Hanle effect. $I^{l,r}$, $Q^{l,r}$ and $\delta^{l,r}$ correspond to the I, Q and δ signals on the left and right sides of the array. They need not be identical due to pixel misalignments. If following Donati et al. (1990) we assume that $Q_j \ll I_j$, neglect pixel mismatch, i.e. assume that $I_j^r = I_j^l$, $Q_j^r = Q_j^l$ and $\delta_j^r = \delta_j^l$, and perfect modulation, then we obtain

$$F = \frac{Q_1 + \delta_1}{I_1} + \frac{Q_2 + \delta_2}{I_2}, \tag{4}$$

which, except for the cross-talk terms neglected by Donati et al. (1990), Semel et al. (1993) and Semel (1994, 1995) is identical to the result of these authors. The important point stressed by Semel and co-workers is that F is independent of R_j and of $G_{l,r}$, making it unnecessary to flat-field and allowing noise levels to be reached in Q/I that lie substantially below those normally achieved with flat-fielding, as Semel et al. (1993) demonstrated for stellar data. In the following we continue to neglect pixel mismatch, imperfect modulation, etc.

3.2.2. Extension to larger polarisation signals

The method of Semel et al. (1993) works well as long as the actual Q/I signal is small. This is due to the fact that they use a linearisation based on the assumption that $Q/I \ll 1$. This assumption introduces significant systematic errors (i.e. errors larger than 10^{-3}) for Q/I signals larger than 1–2%. This means that for scattering polarisation measurements on the Sun this method is restricted to large μ only, or to spectral lines that have intrinsically very low polarisation. This is, given the promise of the method, a very unsatisfactory situation, in particular for the blue and UV, where currently no other instrument is available that can achieve the desired accuracy. In the following we describe some attempts to improve it.

F can be rewritten in terms of

$$\epsilon = \frac{Q_1 + \delta_1}{I_1} + \frac{Q_2 + \delta_2}{I_2} \tag{5}$$

and

$$a = 1 + \frac{Q_1 + \delta_1}{I_1}\frac{Q_2 + \delta_2}{I_2}, \tag{6}$$

giving

$$F = \frac{1}{2}\left(\frac{a+\epsilon}{a-\epsilon} - 1\right) = \frac{\epsilon}{a-\epsilon}. \tag{7}$$

The usual approach is to expand this for $\epsilon < 1$, which gives us

$$F = \frac{\epsilon}{a} + \frac{\epsilon^2}{a^2} + \frac{\epsilon^3}{a^3} + O\left(\frac{\epsilon^4}{a^4}\right), \tag{8}$$

where the symbol O signifies "on the order of". Eq. (8) is a cubic equation in (ϵ/a). However, the desired quantity is ϵ. If we note that $F = O(\epsilon)$ for not too large ϵ, that $a = 1 + O(\epsilon^2)$ and keep only terms to second order in ϵ, then we can solve Eq. (8) for ϵ to get

$$\epsilon = \frac{1}{2}(-1 + \sqrt{1 + 4F}). \tag{9}$$

Similarly the third order approximation, i.e. taking all terms in Eq. (8) up to $O(\epsilon^3)$ into account, is relatively straightforward to write down. However, it is also possible to obtain an exact solution of Eq. (7) if we assume that

$$a = 1 + \epsilon^2/4, \tag{10}$$

which is exactly fulfilled for the case when

$$\frac{Q_1 + \delta_1}{I_1} = \frac{Q_2 + \delta_2}{I_2}. \tag{11}$$

The exact solution then reads:

$$\epsilon = \frac{2}{F}(1 + F - \sqrt{1 + 2F}). \tag{12}$$

Of course, if Eq. (10) is not fulfilled then Eq. (12) is only an approximate solution of Eq. (7) whose accuracy needs to be verified. Note that for $F \to 0$ Eq. (12) becomes singular. Thus for sufficiently small F (a good choice is $F < 0.001$, as tests have shown) the solution assuming $a = 1$ is more stable and just as accurate:

$$\epsilon = \frac{F}{F+1}. \tag{13}$$

Note also that Eqs. (7) and (12) are only valid if $\epsilon < 2$, whereas physically $\epsilon = 2$ is allowed. For resonant scattering this last caveat is of academic interest only.

Tests of the various approximations and the exact solution made using artificial data show that the exact solution is always superior to the expansion solutions, although it too loses accuracy as the difference between $(Q_1 + \delta_1)/I_1$ and $(Q_2 + \delta_2)/I_2$ increases. However, for the observed Q/I values of Ca I 4227 Å (which are smaller than 5%) the accuracy is sufficient (i.e. the errors are smaller than 10^{-4}) even in the extreme case when one of the measurements is zero, e.g., $(Q_2 + \delta_2)/I_2 = 0$.

3.3. Determination of stray light and spectral smearing

The magnitude of the spectral stray light and the spectral resolution are determined by comparing the completely reduced Stokes I profiles observed at disc centre, $I_{\rm obs}$, with a Fourier Transform Spectrum (FTS) obtained by Neckel (1994). The FTS profiles, $I_{\rm FTS}$, are broadened and shifted by various amounts until the two profiles agree.

An intensity profile observed by us can be expressed in terms of an FTS profile by

$$I_{\rm obs} = I_{\rm FTS} \otimes P_I + I_s. \tag{14}$$

Here $\otimes$ signifies convolution, P_I is the instrumental profile (a Gaussian is used, with the Doppler velocity $v_{\rm D}$ as free parameter) and I_s is the stray-light intensity. After continuum normalization we obtain

$$\frac{I_{\rm obs}}{I_{c,\rm obs}} = \left(\frac{(I_{\rm FTS} \otimes P_I)}{I_{c,\rm FTS}} + \frac{I_s}{I_{c,\rm FTS}}\right)\frac{I_{c,\rm FTS}}{I_{c,\rm obs}}, \tag{15}$$

where $I_{c,\mathrm{obs}}$ and $I_{c,\mathrm{FTS}}$ are the continuum intensities. Making use of $I_{c,\mathrm{obs}} = I_{c,\mathrm{FTS}} + I_s$ we rewrite Eq. (15) to

$$\frac{I_{\mathrm{obs}}}{I_{c,\mathrm{obs}}} = \left(\frac{I_{\mathrm{FTS}} \otimes P_I)}{I_{c,\mathrm{FTS}}} + \frac{I_s}{I_{c,\mathrm{FTS}}}\right)\left(1 + \frac{I_s}{I_{c,\mathrm{FTS}}}\right)^{-1}. \quad (16)$$

The profile corrected for stray light becomes

$$\left(\frac{I}{I_c}\right)_{\mathrm{corr}} \equiv \frac{(I_{\mathrm{FTS}} \otimes P_I)}{I_{c,\mathrm{FTS}}} = \frac{I_{\mathrm{obs}}}{I_{c,\mathrm{obs}}}(1 + \frac{I_s}{I_{c,\mathrm{FTS}}}) - \frac{I_s}{I_{c,\mathrm{FTS}}}. \quad (17)$$

Introducing the relative amount of stray light, $s = I_s/I_{c,\mathrm{FTS}}$, we can then write

$$\left(\frac{I}{I_c}\right)_{\mathrm{corr}} = (1+s)\frac{I_{\mathrm{obs}}}{I_{c,\mathrm{obs}}} - s\ . \quad (18)$$

Similarly, using

$$Q_{\mathrm{obs}} = Q_{\mathrm{corr}} + kI_{\mathrm{obs}} \quad (19)$$

one can derive

$$\left(\frac{Q}{I}\right)_{\mathrm{corr}} = \left(\frac{Q_{\mathrm{obs}}}{I_{\mathrm{obs}}} - k\right)\frac{I_{\mathrm{obs}}}{I_{\mathrm{obs}} - I_{c,\mathrm{obs}}\, s/(1+s)}\ , \quad (20)$$

where k is the fraction of the intensity, including the stray light, which is added to the intrinsic Q. In Q/I it represents a zero-line offset, being to first order spectrally flat. Typical values found for our observations are $v_{\mathrm{D}} = 1.2$ km s^{-1}, which corresponds to 17 mÅ, and $s = 1\%$. s is sufficiently small to make second order effects negligible.

3.4. Determination of the polarisation zero level

For symmetry reasons Q/I due to resonance polarization is expected to be zero at solar disc centre. Any Q/I signal seen in such (disc centre) recordings is therefore due to instrumental polarisation or the Zeeman effect. The latter can easily be avoided by measuring in the quiet Sun and moving the telescope. We nevertheless find a sinusoidal fixed-pattern in Q/I with an amplitude of about 0.1%. We believe that the origin of this sinusoidal signal lies in the half-wave plate, since for other projects we measured V/I Stokes signals with a quarter-wave plate and we found no sinusoidal signal at sun centre. Note that exactly the same fixed pattern is also present in the recordings made near the limb, as is best seen when considering a relatively narrow line like Sr I 4607 Å. Therefore, to correct our data for this fixed-pattern background, Q/I recorded at solar disc centre is subtracted from limb recordings. As a consequence the parameter k in Eq. (20) is eliminated or at least significantly reduced. The zero level of the polarisation is determined from the resulting Q/I polarisation in the cores of the depolarising blends at 4225.96 Å, 4226.43 Å, 4227.34 Å and 4227.43 Å in the wings of Ca I 4227 Å. In the cores of these blends Q/I is expected to be a fraction (corresponding to the blending line's relative rest intensity) of the continuum polarisation. In the cases in which the continuum polarisation was not co-temporally measured we used the average continuum polarisation at the corresponding μ value. Although the accuracy of the polarisation zero level derived in these cases is somewhat lower, tests have shown the reduction in accuracy to be small. In general, the observed values of the blend line-to-continuum polarisation ratio (after subtraction of disc centre values) showed good agreement with the expected ratios, without having to introduce a non-zero k in Eq. (20). Only in 22 cases out of a total of 207 was a non-zero value of k needed. In these cases k varied between 0.05% and 0.5%, with a mean value of $k = 0.2\%$. The reason for these non-zero k values is unclear. Nevertheless, we retained these 22 recordings in our data, since they exhibit no other anomalies. Their results also agree well with those of the other 185 spectra. In Fig. 1 we show a reduced recording of a CLV. Illustrated is a typical case with no zero-line correction having to be introduced.

We find that the alignment of the predisperser is a critical source of errors in the zero level. Observations with imperfect alignment turned out to require anomalously large k values to correct. These recordings were removed and are not counted among the 207 Q/I spectra used in the further analysis.

3.5. Noise reduction: Fourier smoothing

After the reductions described so far each recording consists of approximately 100 I and Q/I spectra at different spatial positions along the slit. In order to reduce the noise we first add all the spectra along the slit together, leading to a single I and Q/I spectrum per recording. This means that we refrain, in the present paper, from detecting any variations in Q/I on scales below 20″. Finally, we smooth the Q/I spectrum by applying a low-pass filter to its Fourier transform. The efficiency of the Fourier filtering technique is illustrated in Fig. 1b. An unfiltered, but spatially averaged Stokes Q/I profile is plotted in Fig. 1b. It has been shifted downward for clarity. The corresponding FFT smoothed profile is the solid profile with the smallest amplitude ($\mu = 0.4$) in Fig. 1b. Fourier smoothing also allows us to estimate the residual noise in a straightforward manner. We find 2–3$\times 10^{-4}$ for the residual noise in units of I_c.

4. Analysis and results

4.1. The Q/I profile

In Fig. 1 we show an example of the CLV of the fully reduced Stokes Q/I (Fig. 1b) as well as the corresponding I/I_c profile at two μ values (Fig. 1a). The dotted I/I_c profile refers to a measurement at $\mu = 0.1$, the solid profile to disc centre. Note the significant weakening of the line from disc centre to the limb. The quantitative agreement of the Stokes I CLV with the observations of Stenflo et al. (1980) is excellent.

The 3 principal blends at 4225.96 Å, 4226.43 Å and 4227.43 Å are due to iron lines.

The Q/I profiles in Fig. 1b were obtained at $\mu = 0.1$, 0.15, 0.2, 0.3 and 0.4 (from top to bottom). The downward shifted unsmoothed curve for $\mu = 0.4$ has already been discussed in Sect. 3.5. The typical features of the Ca I 4227 Å Q/I spectral profile (the narrow peak in the core and the 2 strong peaks in the wings) and the rapid increase of the polarisation towards

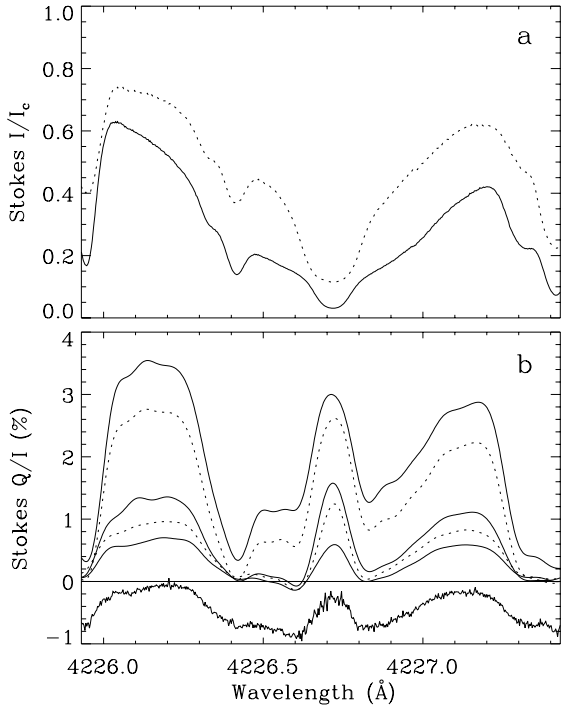

Fig. 1. a Stokes I/I_c spectra of Ca I 4227 Å, where I_c is the continuum intensity. The solid profile was observed at $\mu = 1$, the dotted profile at $\mu = 0.1$. **b** Stokes Q/I spectra, where Q is net linear polarisation (parallel to the limb minus perpendicular to the limb). The top 5 spectra were obtained at (from top to bottom) $\mu = 0.1$, 0.15, 0.2, 0.3 and 0.4. The noisy spectrum at the bottom of the frame is the same as the spectrum at $\mu = 0.4$, but prior to Fourier smoothing. It has been shifted downwards by 0.75% for clarity.

the limb are clearly seen and are also found in all other CLV series. They agree qualitatively with previous observations. Other, lesser spectral features are found in many, but not all spectra. An example is the slightly negative Q/I seen in Fig. 1b at 4226.6 Å (i.e., net linear polarisation perpendicular to the limb). It increases with μ until $\mu = 0.4$ and decreases again towards higher μ (not plotted). This effect and others of similar magnitude do not influence our conclusions in any way.

A theoretical understanding of the wing polarisation of Ca I 4227 Å was first provided by Dumont et al. (1973). Later Rees & Saliba (1982) and Saliba (1985) showed how the presence of a narrow polarisation peak in the Doppler core together with the separate peaks in the wings could be understood as an effect of partial frequency redistribution in polarized radiative transfer for strong lines (cf. also Frisch 1996).

Inspection of Fig. 1b directly reveals that the line core and the line wings do not exhibit the same CLV. While the wing polarisation increases in regular steps between $\mu = 0.4$ and 0.2, the line core polarisation makes a large jump between $\mu = 0.4$ and 0.3, but is practically unchanged between $\mu = 0.3$ and 0.2. Also, the maximum line core polarisation is smaller than the maximum blue-wing polarisation in 3 of the 5 plotted spectra. This is in stark contrast to the Q/I FTS spectrum of this line plotted by Stenflo et al. (1983b) and to a certain extent also to the results of Stenflo et al. (1980), who find a considerably higher line-core than blue-wing peak.

4.2. Parameters of the Q/I profile

In the following we quantify these differences in behaviour between core and wing. To this end we determine the following three parameters of the Q/I profile: The maximum Q/I value in the blue wing (i.e. at $\lambda < 4226.5$ Å), in the red wing ($\lambda > 4226.9$ Å) and in the line core. In the following we simply refer to these parameters as blue-wing, red-wing and line-centre Q/I, or $(Q/I)_b$, $(Q/I)_r$ and $(Q/I)_c$, respectively.

In Fig. 2 the CLV of blue-wing and line-centre Q/I of Ca I 4227 Å are plotted. The two most obvious trends are the expected increase of Q/I towards the limb, and the increase of the scatter of *a priori* unknown origin. An analysis of the noise and uncertainties in the line profiles suggests that this increased scatter is not just due to instrumental noise. A major observational uncertainty is the value of μ, which due to the steep CLV of Q/I near the limb leads to a larger scatter there.[2] The rectangles in Fig. 2a represent the error boxes of the mean Q/I values at each μ. The solid curve in Fig. 2a is a fit to the boxes with a function of the form

$$\frac{Q}{I} = \frac{a(1-\mu^2)}{(\mu + b)}, \tag{21}$$

where $a = 0.4\%$ and $b = 0.05$ are the best-fit parameters. The choice of this functional form, first introduced by Stenflo et al. (1997), is based on two main considerations. Firstly, in the case of a plane-parallel stratification, the path length of an optically thin layer scales as $1/\mu$. Secondly, the source function of Stokes Q scales as $(1 - \mu^2)$. Combining these two dependences we get the form $(1 - \mu^2)/\mu$, which gives a good description for optically thin lines. We can still use it to approximate the CLV of optically thick lines by introducing the free parameters a and b. Parameter b enables us to better account for the breakdown of the plane-parallel approximation when approaching the limb.

The line-centre Q/I, plotted in Fig. 2b, shows a CLV similar to the blue wing, but with larger scatter. We could find no instrumental reason for this increased scatter and conclude that it is of solar origin. As compared with the CLVs published by Stenflo et al. (1980) our blue-wing Q/I values are about 20% larger, while the line-centre values are smaller, in particular at large μ (the two data sets agree better near the limb, but the error bars and the scatter are also larger there).

The difference in behaviour between line centre and wings is much clearer when one eliminates μ by plotting $(Q/I)_r$ and $(Q/I)_c$ vs. $(Q/I)_b$. In Fig. 3a we show red-wing Q/I vs. blue-wing Q/I (with each spectrum again being represented by a

[2] Note that even if μ does not suffer from systematic errors, some scatter is introduced by image motion into Q/I. The μ value may change significantly in an exposure close to the limb lasting several seconds. Since the CLV of Q/I is strongly non-linear near the limb, an average over Q/I obtained at different μ values is not the same as the Q/I measured at the average μ value.

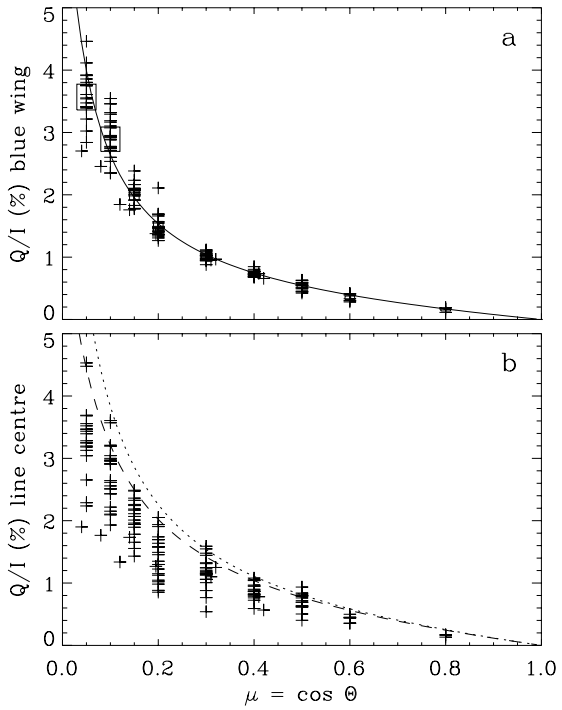

Fig. 2a and b. Centre-to-limb variation (CLV) of the maximum Q/I in the blue wing (Fig. 2a) and in the line core (Fig. 2b). Each plus represents a different spectrum. In Fig. 2a the rectangles represent the error boxes of the average of Q/I for all the observations at a given μ, while the curve is an analytical fit to these average values. In Fig. 2b the dotted and dashed curves are upper envelopes to the data points (see text for details)

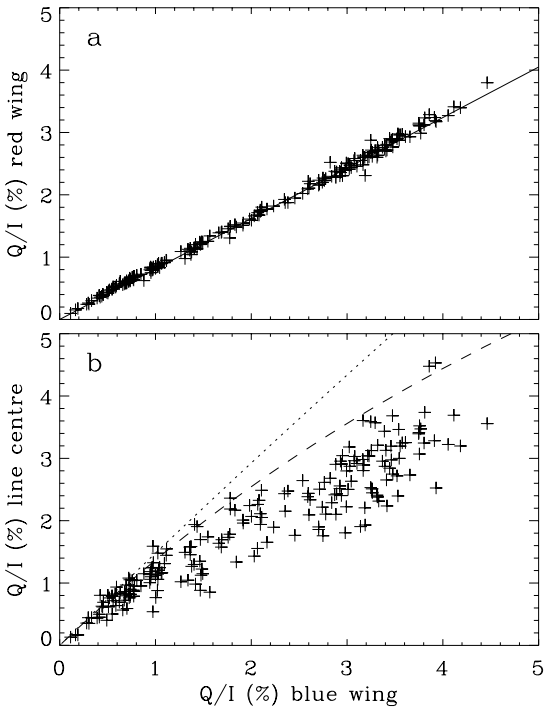

Fig. 3a and b. Red-wing Q/I (Fig. 3a) and line-centre Q/I (Fig. 3b) vs. blue-wing Q/I. The straight line in Fig. 3a is a linear fit to the data, the dotted and dashed curves in Fig. 3b are envelopes to the data points corresponding to those plotted in Fig. 2b

plus). The relationship between the Q/I of the two wings remains remarkably linear over almost 2 orders of magnitude and a large range of μ values. It can be described by the linear regression passing through the origin (in units of % polarisation)

$$(Q/I)_r = 0.81(Q/I)_b \ , \tag{22}$$

which is also plotted. Even more remarkable is the small scatter exhibited by the data points. The standard deviation of the points around this regression is 0.0543 and is a measure of the total uncertainty in the line parameters. This value is less than twice the value expected from the instrumental noise, which suggests that the profile shape in the wings is extremely stable. The tight relationship seen in Fig. 3a also confirms our suspicion that most of the scatter seen in Fig. 2a is merely due to uncertainties in μ.

Fig. 3b, in which the line-centre Q/I is plotted vs. blue-wing Q/I, shows a very different picture. The scatter is very large, much larger than what any observational uncertainties could be expected to introduce. We must therefore search for a solar source of this scatter. The most likely source is the Hanle effect, since it acts almost exclusively on the line core, while leaving the wings unaffected. In the presence of a magnetic field the Hanle effect depolarizes the line core and rotates the direction of linear polarisation, as was first observed for the Ca I 4227 Å line by Stenflo (1982) . The depolarisation depends on the strength and direction of the magnetic field. Therefore a magnetic field that varies spatially in strength or direction can produce a scatter in the core-to-wing Q/I ratio, since we randomly sample solar locations with different field strengths or directions.

Without any further analysis we can immediately conclude that the field whose influence we are observing is relatively weak (since it does not completely destroy the resonance polarisation), and that it is chromospheric (since the core of Ca I 4227 Å is formed in the lower or middle chromosphere).

Interestingly, $(Q/I)_c$ is of approximately the same magnitude as $(Q/I)_b$. This is better seen in Fig. 4, in which the $(Q/I)_c$ to $(Q/I)_b$ ratio is plotted vs. μ. Although this ratio lies around unity, it does (in its average values, given by the error boxes) show a trend with μ, namely a decrease towards the limb (if we disregard the box at $\mu = 0.8$, since only three observations contribute to it, each with a $Q/I < 0.1\%$).

4.3. Depolarisation and field strength

The next step is to quantify the Hanle depolarisation and finally use it to determine the field strength. The main hurdle is estimating the Q/I that one would measure in the complete absence of a weak chromospheric field. Faurobert-Scholl (1992, 1994) estimated this quantity from radiative transfer calculations of the line profile in an atmosphere of the field-free quiet Sun. Here

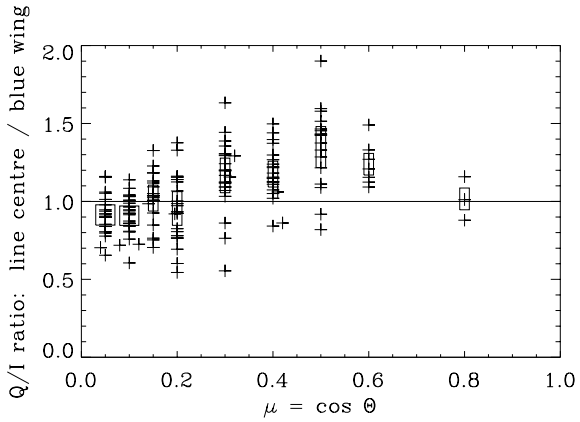

Fig. 4. CLV of the line-centre to blue-wing Q/I ratio. Rectangles represent the error boxes of the average ratios at each μ

we make use of the large number of observations that we have and attempt a model-independent estimate. We take a conservative approach and assume that there are some locations on the Sun which are practically field-free (in the sense that the Hanle depolarisation is negligible). An upper envelope to the data points in Fig. 2b can thus be taken to represent the field-free CLV of the line core Q/I. For this envelope we choose the analytical form given by Eq. (21), which already successfully described the CLV of $(Q/I)_b$, as well as the Q/I CLV of Sr I 4607 Å (Stenflo et al. 1997). Even after restricting ourselves to this choice the exact shape of the envelope (or equivalently the values of a and b) is not obvious. In Fig. 2b we have selected two envelopes that appear reasonable. They are represented by the dotted and dashed curves, which have the parameter values $a = 0.6\%$, $b = 0.055$ and $a = 0.6\%$, $b = 0.085$, respectively. We determine the field strength for both these estimates, which allows us to judge the uncertainty in the field strength introduced by the uncertainty inherent in this estimate.

The synthetic line-center Q/I values calculated for a field-free atmosphere by Faurobert-Scholl (1992) lie closer to the dotted envelope – with which they agree very well – so that the results obtained using it are probably more reliable. Unfortunately, the profiles of Faurobert-Scholl (1992) have not been broadened to take into account spectral smearing or macroturbulent velocity broadening, so that we carry out the analysis using both envelopes.

Next, by forming the ratios between the curves in Fig. 2b and the solid curve in Fig. 2a we obtain the 2 envelopes (dotted and dashed curves) in Fig. 3b. As in Fig. 2b the dashed curve lies closer to the data points and is a good estimate of a tight envelope (within the uncertainty due to noise). The dotted curve, on the other hand, almost corresponds to a straight line in Fig. 3b, which also appears reasonable in view of the strictly linear relationship between Q/I of the red and blue wings displayed in Fig. 3a. According to this choice we assume that the core-to-wing ratio of Q/I produced by resonant scattering (in the absence of a magnetic field) is nearly independent of μ,

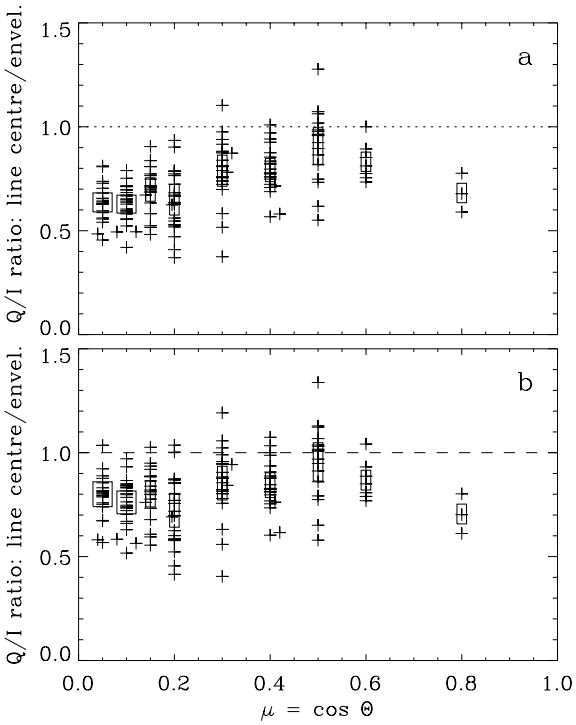

Fig. 5a and b. The ratio of line-centre Q/I to its envelope vs. μ. The plotted ratio is a measure of the relative depolarisation. **a** The dotted curve in Fig. 3b is used as envelope, **b** the dashed curve in Fig. 3b is used. Error boxes for the average values are also plotted

whereas for the dashed curve the ratio decreases towards the limb.

The main diagnostic of the magnetic field is the fractional depolarisation it causes, i.e. the ratio between line-core Q/I and its envelope. In order to suppress the additional scatter introduced by uncertainties in μ we form this ratio for each given blue-wing Q/I. The ratio is then free from uncertainties in μ. It can nevertheless depend on μ. Consquently, we plot it vs. μ in Fig. 5. Fig. 5a shows the depolarisation obtained by employing the dotted envelope, Fig. 5b that resulting from the dashed envelope.

We can now calculate the strength of the magnetic field responsible for the Hanle depolarisation plotted in Fig. 5. A detailed description and derivation of the theory underlying such calculations for different field-strength distributions has been given by Stenflo (1982, 1987, 1994, chapter 10) and Landi Degl'Innocenti (1985, 1988). Since we have no information on Stokes U (which is needed to distinguish between different configurations of a field that is homogeneous within the spatial resolution element) we prefer to simply consider a turbulent field. We must distinguish between an isotropically turbulent magnetic field and what we shall call a canopy field, since they give different field strengths. In the former case it is assumed that the magnetic field distribution is isotropic, i.e. it is randomly oriented at scales smaller than the spatial resolution element. For the canopy case, it is assumed that the field is horizontal

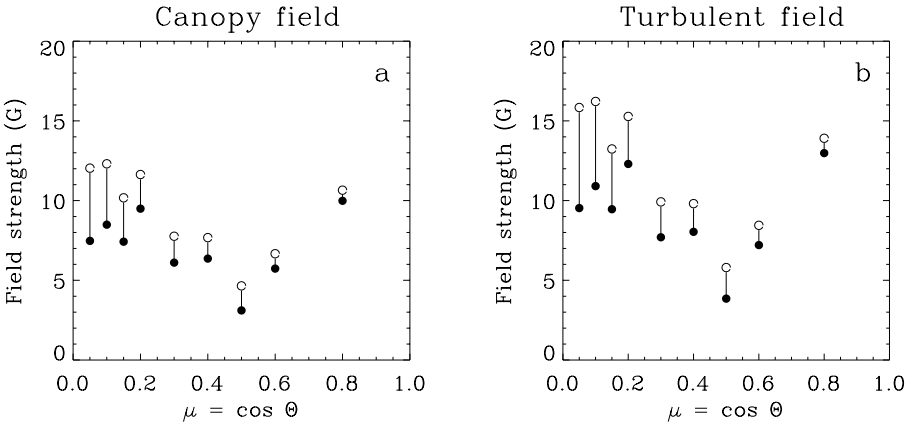

Fig. 6a and b. CLV of the field strength derived from the average relative depolarisation at different μ values. Filled circles: value resulting when the dashed envelope in Fig. 3 is chosen. Open circles: value resulting from choosing the dotted envelope. **a** Results of assuming a purely horizontal canopy field, **b** results of an isotropic, "turbulent" field

and randomly oriented in azimuth. In both cases the magnetic field is assumed to be homogeneous in strength over a spatial resolution element, although it varies in direction. The rationale behind using both distributions is that as long as we do not have additional information on the magnetic geometry we consider both, in order to judge the uncertainties. We do, however, from both Zeeman effect observations (Giovanelli & Jones 1982) and magnetohydrostatic models (Solanki & Steiner 1990) expect the field in the mid chromosphere to be relatively canopy-like.

Following Stenflo (1982,1994), the Hanle depolarisation, k_H, i.e. the ratio between Q/I at line centre and its envelope, can be written as

$$k_H^{\text{canopy}} = 1 - 0.75 \sin^2 \alpha_2 \tag{23}$$

in the case of a canopy field, and as

$$k_H^{\text{turbulent}} = 1 - 0.4(\sin^2 \alpha_1 + \sin^2 \alpha_2) \tag{24}$$

in the case of a turbulent field. The Hanle mixing angles α_1 and α_2 are given by

$$\tan \alpha_K = \frac{KB}{B_0/k_c^{(K)}}, \tag{25}$$

where $K = 1$ or 2, B is the field strength, $k_c^{(K)}$ is the collisional branching ratio for the $2K$-multipole ($k_c^{(1)} \approx k_c^{(2)}$) and B_0 is the "characteristic field strength" for the Hanle effect. From Stenflo (1982) we obtain for Ca I 4227 Å: $B_0/k_c^{(K)} = 24.8$ G. In general Eqs. (23) and (24) result in different values for B.

We apply Eqs. (23)–(25) to the depolarisations plotted in Fig. 5 and obtain four possible values of B for each observed spectrum; two from the combination of Eq. (23) with each of the two envelopes and similarly two from Eq. (24). The results are plotted in Fig. 6; filled circles refer to data calculated with the dashed envelope from Fig. 3b, open circles refer to the dotted envelope.

As expected, the dotted envelope gives larger field strengths by approximately 10–60%. The difference between the results obtained with the two envelopes is largest near the limb since they also differ most strongly from each other there.

There is also a systematic difference between the field strength of a turbulent field and of a canopy field, with the former having to be on average 30% larger in order to produce the same depolarisation.

The uncertainties due to the effects mentioned above are found to be the dominant source of the difference in the field strength values derived at a given μ. Photon noise only becomes a significant source of error at $\mu > 0.8$.

Keeping all the uncertainties in mind we can nevertheless say that the field strength of the detected canopy fields is on the order of 10 G. More specifically it lies within the range 5–15 G. If we once again neglect the point at $\mu = 0.8$ (due to the low S/N and the poor statistics) then there appears to be a trend towards larger field strengths closer to the limb. Due to the better agreement of the dotted envelope given in Fig. 2b with the theoretical predictions of Faurobert-Scholl (1992) we expect that the higher field-strength values (open circles in Fig. 6) are more realistic.

So far we have only considered the average depolarisation at any given μ. The scatter in the depolarisation values of the individual data points is considerably larger than the estimated errors. We therefore expect that most of this scatter is due to a distribution of the magnetic field strength of the canopy; each location on the Sun having a somewhat different field strength (or alternatively a different direction; we shall not follow this possibility further, however). In the following we therefore determine the field strength from each spectrum individually, obtaining 207 B values. Note that there are some points with negative depolarisation, possibly due to noise, or to small errors in the choice of the envelope. For these anomalous points we have set the field strength to zero. Histograms of the field strength are plotted in Fig. 7. The two plotted histograms represent the extremes of the four possible histograms arising from the different combinations of turbulent and canopy field, with the dotted and dashed envelopes in Fig. 3. Note that both histograms are relatively symmetric around their mean and broad, with FWHM roughly the value of the average field strength. In this sense the two histograms differ mainly in the value of the average field strength 7.5 G and 14 G, respectively. These values are to be compared with 7 G and 12.5 G, obtained by averaging the

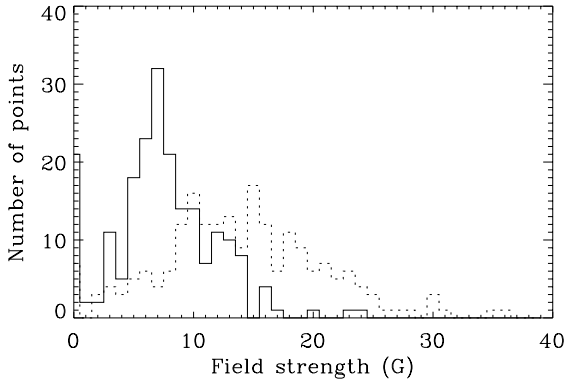

Fig. 7. Histogram of magnetic field strengths. Solid line: histogram obtained by assuming a canopy field and a depolarisation arising from the use of the dashed envelope in Fig. 3. Dotted line: turbulent field and dotted envelope.

field strengths at the different μ values in Fig. 6 (filled circles in Fig. 6a and open circles in Fig. 6b, respectively). Note, that when carrying out this averaging we have weighted the individual μ values by the number of observations underlying each.

5. Discussion and conclusions

We have presented low-noise ($2–3\times10^{-4} I_c$) observations of Q/I at over 200 locations on the quiet Sun. The present data hence not only have lower noise, but also represent a much larger statistical sample of the solar surface than previous data sets. From these observations we derive many CLVs of the scattering polarisation of this line. We find that while the ratio of blue- to red-wing polarisation remains strictly constant, the line core shows a large scatter relative to the wings. This scatter is much larger than expected from the error budget. It is best interpreted in terms of Hanle depolarisation by a weak field. Using an empirical estimate of the field-free line-core Q/I of this line as suggested by our data, we find that a field strength of 5–15 G is required to explain the observations. This field strength refers to the height of formation of the Ca I 4227 Å line core, approximately 800–1000 km above $\tau_{5000} = 1$ (Faurobert-Scholl 1992). The different field-strength values partly refer to different μ values (there is a trend, although not a very clear one, for the field strength to increase towards the limb). A large fraction of the uncertainty in the derived field strength stems, however, from the ambiguity in the assumed magnetic geometry and the uncertainty in the estimated CLV of the line core Q/I in the absence of magnetic fields.

Chromospheric field strengths have earlier been derived from the Hanle depolarisation of this line by Faurobert-Scholl (1992) from observations made near the solar limb by Stenflo et al. (1980). She found values between approximately 20 and 100 G, with the spread being due to different assumptions on the field geometry (canopy base height, width of canopy base, inclination of the field). These values are larger than the ones we have derived in the present paper. We identify four possible sources of the discrepancy.

1.Our estimate of the depolarisation is too conservative.

2.The field strengths derived by Faurobert-Scholl are too large, possibly due to errors in the observations they are based on, or due to sampling of non-typical solar regions. While our field strengths are based on averages of many observed CLVs, the previously derived field strengths were based on one single CLV.

3.The difference is due to the different magnetic field structures assumed in the two investigations. While our simple analytical determinations assume a height-independent field strength, Faurobert-Scholl considers a canopy field which changes in strength over the height range of line core formation, and she numerically solves the transfer problem.

4.The quiet sun chromospheric fields have changed between the times at which our observations and those of Stenflo et al. (1980) were obtained.

Some comments to the above points: Possibility 1 is plausible, since our conservative estimate is based on the assumption that there is no depolarisation in at least some of the data, i.e. some parts of the solar surface are free from detectable fields in chromospheric layers. This need not be correct.

Concerning possibility 2, a comparison between our observations and those of Stenflo et al. (1980) shows that relative to the line wing polarisation our line-centre polarisation is lower, in particular at large μ values. Interestingly, it was exactly at these μ that the observations of Stenflo et al. (1980) showed Q/I values significantly larger than those calculated in a standard atmosphere in the absence of a magnetic field (Faurobert-Scholl 1994). Our observations should therefore reduce the discrepancy between observations and theory.

The true source of the discrepancy can only be definitely identified by comparing our observations with model calculations, such as those of Faurobert-Scholl (1992, 1994).

Acknowledgements. We thank H. Lin for useful discussions on the data reduction and M. Faurobert-Scholl for helpful comments on the interpretation. Many people have helped to refurbish the instrumentation at IRSOL. We gratefully acknowledge their contributions, in particular those of E.Alge, K.H. Duensing, G. Küveler, E. Wiehr and A.D. Wittmann. We are greatly indebted to P.T. Utermöhlen (†1992) and A. Rima, who organized the financial aspects and directed the refurbishment. Financial support has been provided by the canton of Ticino, the city of Locarno and the ETH Zürich.

References

Bommier V., 1980 A&A 87, 109
Brückner G., 1963 Z. Astrophys. 58, 73
Donati J.-F., Semel M., Rees D.E. et al., 1990, A&A 232, L1
Dumont S., Omont A., Pecker J.C., 1973 Sol. Phys. 28, 271
Faurobert-Scholl M., 1992 A&A 258, 521
Faurobert-Scholl M., 1993 A&A 268, 765
Faurobert-Scholl M., 1994 A&A 285, 655
Faurobert-Scholl M., Feautrier N., Machefert F. et al., 1995 A&A 298, 289
Frisch H., 1996 Sol. Phys. 164, 49

Hanle W., 1924 Z. Phys. 30, 93
Giovanelli R.G., 1980 Sol. Phys. 68, 49
Giovanelli R.G., Jones H.P., 1982 Sol. Phys. 79, 267
Landi Degl'Innocenti E., 1982 Sol. Phys. 79, 291
Landi Degl'Innocenti E., 1985 Sol. Phys. 102, 1
Landi Degl'Innocenti E., 1988 A&A 192, 374
Leroy J.-L., Ratier G., Bommier V., 1977 A&A 54, 811
Martínez Pillet V., Sánchez Almeida J., 1991 A&A 252, 861
Moruzzi G., Strumia F. (Eds.), 1991 The Hanle Effect and Level-Crossing Spectroscopy Plenum Press
Neckel H., 1994 The Sun as a Variable Star: Solar and Stellar Irradiance VariationsJ. Pap, C. Fröhlich, H.S. Hudson, S.K. Solanki Cambridge University Press, Cambridge IAU Coll. 143, 37
Povel H.P., 1995, Optical Engineering 34, 1870
Querfeld C.W., Smartt R.N., Bommier V., Landi Degl'Innocenti E., House L.L., 1985 Sol. Phys. 96, 277
Rees D.E., Saliba G.J., 1982 A&A 115, 1
Sahal-Bréchot S., Bommier V., Leroy J.-L., 1977 A&A 59, 223
Saliba G.J., 1985 Sol. Phys. 98, 1
Semel M., 1994 Solar Surface MagnetismR.J. Rutten, C.J. Schrijver Kluwer, Dordrecht, p. 509
Semel M., 1995 3D Spectroscopic Methods in Astronomy G. Comte, M. Marcelin ASP Conf. Ser., Vol. 71, p. 340
Semel M., Donati J.-F., Rees D.E., 1993 A&A 278, 231
Solanki S.K., Steiner O., 1990 A&A 234, 519
Stenflo J.O., 1974 Sol. Phys. 37, 31
Stenflo J.O., 1982 Sol. Phys. 80, 209
Stenflo J.O., 1987 Sol. Phys. 114, 1
Stenflo J.O., 1994 Solar Magnetic Fields: Polarized Radiation DiagnosticsKluwer, Dordrecht
Stenflo J.O., 1997 A&A in press
Stenflo J.O., Keller C.U., 1996 Nat. 382, 588
Stenflo J.O., Keller C.U., 1997 A&A in press
Stenflo J.O., Baur T.G., Elmore D.F., 1980 A&A 84, 60
Stenflo J.O., Twerenbold D., Harvey J.W., 1983a A&AS 52, 161
Stenflo J.O., Twerenbold D., Harvey J.W., Brault J.W., 1983b A&AS 54, 505
Stenflo J.O., Bianda M., Keller C.U., Solanki S.K., 1997 A&A in press
Wiehr E., 1975 A&A 38, 303

This article was processed by the author using Springer-Verlag LaTeX A&A style file *L-AA* version 3.